Talwar et al., J Material Sci Eng 2017, 6:2
DOI: 10.4172/2169-0022.1000324

Journal of Material Sciences & Engineering

Research Article OMICS International

Assessing Biaxial Stress and Strain in 3C-SiC/Si (001) by Raman Scattering Spectroscopy

Talwar DN[1]*, Wan L[2], Tin CC[3] and Feng ZC[2]

[1]*Department of Physics, Indiana University of Pennsylvania, USA*
[2]*Laboratory of Optoelectronic Materials and Detection Technology, Guangxi Key Laboratory for Relativistic Astrophysics, School of Physical Science & Technology, Guangxi University, China*
[3]*Department of Physics, Auburn University, Auburn, USA*

Abstract

Highly strained 3C-SiC/Si (001) epilayers of different thicknesses (0.1 μm-12.4 μm) prepared in a vertical reactor configuration by chemical vapor deposition (V-CVD) method were examined using Raman scattering spectroscopy (RSS). In the near backscattering geometry, our RSS results for "as-grown" epilayers revealed TO- and LO-phonon bands shifting towards lower frequencies by approximately ~2 cm^{-1} with respect to the "free-standing" films. Raman scattering data of optical phonons are carefully analyzed by using an elastic deformation theory with inputs of hydrostatic-stress coefficients from a realistic lattice dynamical approach that helped assess biaxial stress, inplane tensile- and normal compressive-strain, respectively. In each sample, the estimated value of strain is found at least two order of magnitude smaller than the one expected from lattice mismatch between the epilayer and substrate. This result has provided a strong corroboration to our recent average-t-matrix Green's function theory of impurity vibrational modes – indicating that the high density of intrinsic defects at the 3C-SiC/Si interface are possibly responsible for releasing the misfit stresses and strains. Unlike others, our RSS study in "as-grown" 3C-SiC/Si (001) has reiterated the fact that for ultrathin epilayers (d<0.4 μm) the optical modes of 3C-SiC are markedly indistinctive. The mechanism responsible for this behavior is identified and discussed. PACS: 78.20.-e 63.20.Pw 63.20.D.

Keywords: 3C-SiC/Si (001); Raman scattering; Stress and strain; Elastic theory

Introduction

Silicon carbide (SiC) is one of the very few IV-IV compound semiconductors – exhibiting exceptional mechanical, electrical and chemical properties [1-14]. The novel characteristics of SiC have made it suitable for fabrication of many important modern [1-10] devices for microelectronic, optoelectronic and sensor application needs. The scientific interest in SiC is stimulated by a strong chemical bond between Si and C atoms which provides the material a wider-bandgap, extreme hardness, high thermal stability, chemical inertness, higher thermal conductivity, high melting temperature, large bulk modulus, high critical (breakdown) electric field strength, and low dielectric constant. Among other wide-bandgap semiconductors, SiC is rather distinctive for controlling both *n*- and *p*-type dopants [11-18] across the broader concentration range (~10^{14}-10^{19} cm^{-3}). The ability of SiC to form native silicon dioxide (SiO_2) is an advantage [19-21] leading to its use in device fabrications. SiC has also been considered as a substitute for Si to make Schottky diodes and metal–oxide–semiconductor field-effect transistors (MOSFETs) for high-power, high-temperature, and high-frequency applications. Both crystalline and polycrystalline SiC have become attractive in recent years to design micro- and nano-electro-mechanical systems (MEMS, NEMS) [1-10]. While silicon carbide is currently being used to fabricate green, blue and ultraviolet light-emitting diodes (LEDs) – the emerging market [22,23] of utilizing heteroepitaxy/homoepitaxy SiC films is in high-power switches and microwave devices.

SiC occurs in more than 200 different crystalline structures [9-14] called polytypes. While every polytype is perceived by its own stacking sequence of Si-C bilayers – each structure displays its explicit set of distinct electrical and vibrational properties. The customary polytypes that are being developed for commercial needs include the cubic (3C-SiC), hexagonal (4H-SiC, 6H-SiC), and rhombohedral (15R-SiC, 21R-SiC) structures. The original work by Nishino et al [24] proposed a multistep chemical vapor deposition (CVD) method to prepare 3C-SiC on Si. Many attempts have been made in recent years to improve the growth [25-30] mechanisms of 3C-SiC/Si (001) epifilms. The prospect of attaining large area 3C-SiC/Si (001) epilayers by CVD and molecular beam epitaxy (MBE) appears to be very encouraging. Despite the successful growth of 3C-SiC/Si (001) the quality of epilayers is still lacking thus impeding their use in the fabrication of electronic devices. On the other hand, a positive trade-off is its low cost advantage and there is a greater prospect of scalability in the fabrication of devices using Si as compared to 4H-SiC that sustained the current interest in the growth of 3C-SiC/Si for future applications.

There exists a considerable difference in the lattice constants (19.8%) and thermal expansion coefficients (8%) between 3C-SiC and Si. This leads to biaxial strain in 3C-SiC/Si (001) epilayers which might instigate modifying their physical and chemical properties. Whether one will be able to make practical use of such highly strained structures in electronic devices is still an open question. It is quite possible, however, that a large lattice mismatch in 3C-SiC/Si (001) leads to breaking of atomic bonds in epilayers which generates high density of dislocations or intrinsic defects [31]. It is likely that these defects stimulate releasing interfacial strains in epilayers. Therefore, it is imperative to evaluate biaxial stress in 3C-SiC/Si (001) epilayers for further progress in device

***Corresponding author:** Talwar DN, Department of Physics, Indiana University of Pennsylvania, 975 Oakland Avenue, 56 Weyandt Hall, Indiana, Pennsylvania 15705-1087, USA, Tel:7247627719; E-mail: talwar@iup.edu

Received January 28, 2017; **Accepted** February 16, 2017; **Published** February 26, 2017

Citation: Talwar DN, Wan L, Tin CC, Feng ZC (2017) Assessing Biaxial Stress and Strain in 3C-SiC/Si (001) by Raman Scattering Spectroscopy. J Material Sci Eng 6: 324. doi: 10.4172/2169-0022.1000324

engineering. Apart from the x-ray diffraction study (which is insensitive to ultrathin layers) [32,33] the most frequently used technique for stress estimation is the Raman scattering spectroscopy (RSS) [34-46]. Earlier, the method has been used successfully to appraise microstrains in bulk semiconductors under hydrostatic and uniaxial stress [36,37]. As the RSS approach is precise, sensitive, convenient and non-destructive it can be employed for studying the biaxial strain in thin epilayers grown on thick substrates including 3C-SiC/Si (001) [41-45].

The purpose of this work is to explore both theoretically and experimentally the problem of assessing residual stress and strain in 3C-SiC/Si (001) epilayers with large lattice mismatch. By using RSS, we will study the optical phonon shifts in a number of 3C-SiC/Si (001) samples grown by CVD method in the vertical reactor configuration (V-CVD) [30]. A T64000 Jobin Yvon triple advanced research Raman spectrometer, equipped with an electrically cooled charge coupled device (CCD) detector, is employed to measure the optical phonon frequencies in the near backscattering geometry. The observed phonon shifts will be assimilated in a conventional elastic deformation [40-46] theory to appraise the stresses and strains inside the 3C-SiC films. Our calculated biaxial stress in the V-CVD grown 3C-SiC/Si (001) epifilms of varied thickness fall well within the range of 0.45-0.94 GPa, i.e., an order of ~10^9 dyn/cm^2. Theoretical results are compared and discussed with the existing experimental and other simulated data. Despite a considerable difference (~19.8%) in the lattice constants [30] between the bulk Si and 3C-SiC materials – the study has offered significantly lower (two-order of magnitudes) values of inplane strains (i.e., ~0.1-0.2%) as well as normal (i.e., ~-0.07 to -0.14%) strains within the 3C-SiC films grown on Si substrate. While the simulated results are quite surprising – the outcome has undoubtedly offered support to our earlier speculations of high density dislocations and/or intrinsic defects near the 3C-SiC/Si interface [31] which are likely to be responsible for releasing misfit stresses and strains in 3C-SiC films.

Experimental: V-CVD Growth of 3C-SiC/Si (001) Epifilms

3C-SiC epifilms used in the present RSS study are grown on (001) Si substrates under normal atmospheric pressure environment using CVD method in a vertical reactor configuration. Although, we employed 1 in diameter Si wafers as substrates – our reactor is capable of scaling up to handle 3 in diameter Si substrates for growing 3C-SiC epifilms. The V-CVD system utilizes a rotating SiC-coated susceptor heated by a radio-frequency (RF) induction power supply and is capable of operating at atmospheric and low pressure modes. The vertical configuration has several advantages including substrate rotation to give a large-area thickness uniformity, convenient in-situ monitoring of substrate parameters, and easy implementation of various growth enhancement procedures. The method used here to grow 3C-SiC/Si (001) epilayers consisted of three main steps described in details [30] elsewhere. It is to be noted that 3C-SiC/Si (001) epilayers are prepared at 1 atm and 1360°C with source ratio of Si/C (of ~0.33) using growth time τ between 2 min and 4 h at a rate of 3.2 ± 0.1 μm h^{-1} achieving the film thicknesses *d*, between 0.1 μm and 12.8 μm (Table 1). The set of single-crystalline 3C-SiC films used in the RSS study show uniformly smooth and mirror-like surfaces without macro-cracks – even for the thinnest film.

Raman Scattering Spectroscopy

RSS is a powerful and non-destructive technique to provide valuable information on the vibrational characteristics of materials for assessing the epilayer thickness, strain, disorder, and site selectivity of defects [46,47]. The method is particularly suited for probing local atomic- and/or nanoscale structural changes in SiC materials while making careful analysis of its subtle spectral variations. Since RSS efficiency depends upon the polarizability of electron cloud – the process is quite sensitive to light elements involved in producing covalent bonds including SiC. The strong Si-C bonding in 3C-SiC with large bandgap stimulates higher Raman efficiency – requiring incident laser light of visible spectral range with reduced intensity to prevent significant heating of the material samples. We have performed room temperature RSS measurements in the near backscattering $x(y',y')\,\bar{x}$ geometry on several 3C-SiC epifilms of diverse thickness (~0.1 and 12.8 μm) grown on thicker (~200 and 400 μm) Si-substrates. A T64000 Jobin Yvon triple advanced research Raman spectrometer equipped with electrically cooled CCD detector is employed with an Ar^+ 488 nm line as an excitation source, while keeping the power level adjusted to 200 mW.

Sample #	Growth time	Epifilm thickness d μm
125 D	2 min	0.1
125 C	15 min	0.8
125 B	30 min	1.6
125 A	45 min	2.4
119 A	1 hr	3.2
119 B	3 hr	9.6
113	4 hr	12.8

Table 1: Properties of V-CVD grown 3C-SiC/Si (001) samples at 1 atm and 1360°C. The source ratio of Si/C was set at approximately ≅0.33 with different growth times of 2 min, 15 min, 30 min, 45 min, and 1 hr, 3 hr, and 4 hr, respectively.

Assessing the lattice phonons in an ideal backscattering geometry for perfect diamond/zb materials requires strict wavevector conservation [47,48] and polarization selection rules. In the first-order RSS, this constraint limits the phonon wavevector to $\vec{q} = 0$ for observing the lattice modes. Thus, for Si crystal a triply degenerate phonon $\omega_{o(\Gamma)}$ at the center of the Brillouin zone (i.e., Γ-point) is allowed while in 3C-SiC material a doubly degenerate TO mode ($\omega_{TO(\Gamma)}$) is forbidden and a non-degenerate LO phonon ($\omega_{LO(\Gamma)}$) is permitted. By applying the hydrostatic pressure *X* up to 22.5 GPa in bulk 3C-SiC crystals, Raman scattering spectroscopy [37] was used earlier to measure the changes in the long wavelength optical phonon frequencies that helped evaluate the mode Grüneisen parameters γ_H^{TO} and γ_H^{TO} of the optical modes.

Near backscattering Raman spectra to assess stress and strain in 3C-SiC/Si (001)

One must note that the V-CVD grown 3C-SiC/Si (001) epilayers are perceived with biaxial stress in 3C-SiC films due to differences in Si and 3C-SiC lattice constants and thermal expansion coefficients [30]. An elastic deformation theory developed here can be applied to this system for assessing stressess and strains. We used RSS method to study the optical phonon shifts in (*i*) ″as grown″ 3C-SiC epilayers prepared on Si (001) with no processing done after V-CVD growth, and (*ii*) self-supported ″free-standing″ 3C-SiC films in which the Si substrate is removed with KOH etching solution. As an example, we have displayed (Figure 1a and 1b) our results of the RSS measurements recorded in the near back-scattering geometry for a 12.8 μm thick (*a*) "as-grown" and (*b*) "free-standing" film. Clearly, in the "as-grown" sample, the observed $\omega_{LO(\Gamma)}$, $\omega_{TO(\Gamma)}$ modes near ~972 cm^{-1}, ~796 cm^{-1} are seen shifting towards lower frequencies by approximately ~2 cm^{-1} when Si substrate is etched away. In Figure 1a we have also noticed a weak phonon feature appearing between ~938–950 cm^{-1} almost ~20-35

cm^{-1} lower than the $\omega_{LO(\Gamma)}$ phonon line. No such trait emerged, however, in the "free standing" film. By examining several "as-grown" 3C-SiC/Si (001) samples we have realized the weak feature in only a few cases and certainly not in the "free-standing" films. We strongly believe attributing this characteristic to interface states between 3C-SiC and Si. Again, the weak trait has neither affected the $\omega_{LO(\Gamma)}$, $\omega_{TO(\Gamma)}$ phonon lines nor it changed the stress calculations. By using a conventional elastic deformation theory we have evaluated the bi-axial strains in 3C-SiC epilayers by incorporating the observed Raman optical phonon shifts in the "as-grown" and "free-standing" films.

Thickness dependent Raman spectra of 3C-SiC/Si (001)

In Figure 2 we have reported RSS measurements in the near back-scattering geometry for seven of the V-CVD grown 3C-SiC/Si (001) samples (Table 1) in which the film thickness d is varied between 100 Å to 12.8 μm. Except for the 100 Å thick sample, we observed in all other "as-grown" materials (Figure 2) the $\omega_{o(\Gamma)}$ Si phonon line near ~520 cm^{-1} and $\omega_{LO(\Gamma)}$, $\omega_{TO(\Gamma)}$ modes of 3C-SiC near ~972 cm^{-1}, ~796 cm^{-1}, respectively. The relative peak intensities and lineshapes of $\omega_{o(\Gamma)}$ mode for Si substrate and the $\omega_{LO(\Gamma)}$, $\omega_{TO(\Gamma)}$ phonons of 3C-SiC epifilms showed variations with growth time τ or film thickness d. In thicker "as-grown" samples, one expects less penetration of the laser light through 3C-SiC into Si substrate which inflicts a decrease in the intensity of the $\omega_{o(\Gamma)}$ phonon line and a rise of the $\omega_{LO(\Gamma)}$ mode intensity (Figure 2) with respect to $\omega_{TO(\Gamma)}$ phonon. This observation clearly indicates improvement in the crystalline quality of the thicker epilayers prepared with increased growth time τ. Unlike others [44] our RSS study has reiterated (Figure 2) the fact that in "as-grown" samples with thin epilayers (d<0.4 μm) the 3C-SiC optical modes are markedly indistinctive. We will incorporate the observed optical phonon shifts in "as-grown" and "free-standing" films to our elastic deformation theory to estimate both "in-plane" and "normal" strains in epilayers of different thickness.

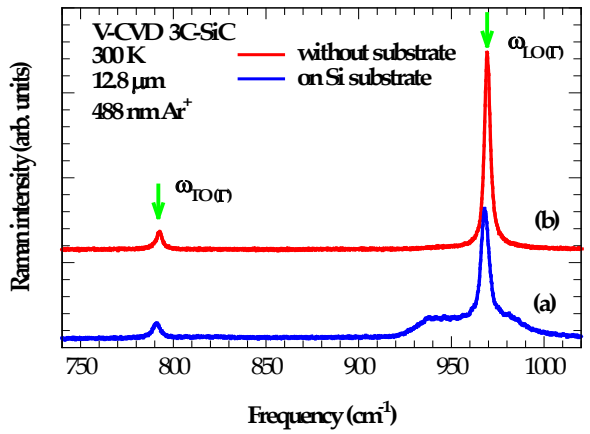

Figure 1: Raman spectra in the near back-scattering geometry of 3C-SiC/Si (sample #113 of film thickness 12.8 μm). An Ar^+ 488 nm line is used as the excitation source while keeping the laser power level adjusted to 200 mW (*a*) blue line on Si substrate and (*b*) redline without Si substrate.

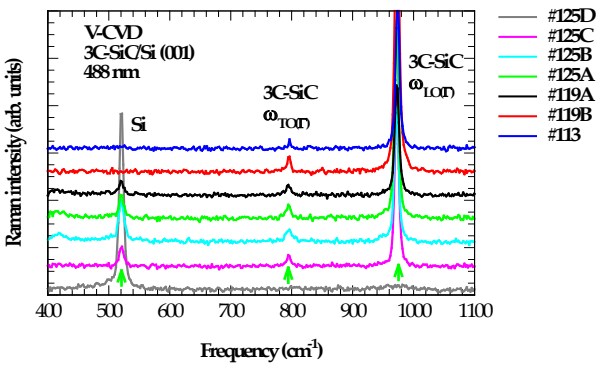

Figure 2: Thickness dependent Raman spectra in the near back-scattering geometry for seven V-CVD "as-grown" 3C-SiC/Si (001) samples, where d is varied between 0.1 μm to 12.8 μm. Except for 0.1 μm thick epifilm, in all other samples we observed $\omega_{o(\Gamma)}$ Si phonon line near ~520 cm^{-1} and $\omega_{LO(\Gamma)}$, $\omega_{TO(\Gamma)}$ modes of 3C-SiC near ~972 cm^{-1}, ~796 cm^{-1}, respectively.

Theoretical Background: Universal Axial Stress and Strain

To comprehend the "pressure-dependent" vibrational properties in semiconductors one can: (i) apply the "hydrostatic pressure" in bulk samples using diamond anvil cell, (ii) perform "uniaxial-stress" on large size specimens, and (iii) examine "biaxial-stress" in thin films prepared on mis-matched substrates. In each case the "pressure" is considerd as a perturbation. By adopting a conventional elastic deformation theory, one can derive expressions for the three cases in terms of Raman-stress coefficients and optical mode frequencies to empathize experimental data.

By using an elasticity theory [49,50] for a continuous media – the strain (ε) and stress (σ) tensors can be linked to the elastic-stiffness $\boldsymbol{C}$ and elastic-compliance $\boldsymbol{S}$ tensors via:

$$\sigma_{ij} = C_{ijkl}\varepsilon_{kl}\,, \tag{1a}$$

$$\text{and} \quad \varepsilon_{ij} = S_{ijkl}\sigma_{kl}\,. \tag{1b}$$

For uniaxial stress, the off-diagonal elements of stress $\sigma_{ij}(i \neq j) = 0$ and strain $\varepsilon_{ij}(i \neq j) = 0$ are zero. In a generalized form, the axial stress and strain tensors are symmetric about the z axis [41]:

$$\sigma = \begin{pmatrix} X & 0 & 0 \\ 0 & X & 0 \\ 0 & 0 & Z \end{pmatrix}, \quad \varepsilon = \begin{pmatrix} \varepsilon_{xx} & 0 & 0 \\ 0 & \varepsilon_{yy} & 0 \\ 0 & 0 & \varepsilon_{zz} \end{pmatrix} \tag{2}$$

In Eq. (2), if X or Z<0 the stress is compressive and it is tensile when X or Z>0. The elements of strain tensor can be rewritten as $\varepsilon_{xx} = \varepsilon_{yy}(=\varepsilon_{\parallel})$ and $\varepsilon_{zz}(\equiv \varepsilon_{\perp})$. Again, one can separate the axial stress into a hydrostatic term X and a uniaxial term P along the z-axis:

$$\begin{pmatrix} X & 0 & 0 \\ 0 & X & 0 \\ 0 & 0 & Z \end{pmatrix} = \begin{pmatrix} X & 0 & 0 \\ 0 & X & 0 \\ 0 & 0 & X \end{pmatrix} + \begin{pmatrix} 0 & 0 & 0 \\ 0 & 0 & 0 \\ 0 & 0 & P \end{pmatrix} \tag{3}$$

with $Z = X + P$. By using Eqs. (1 and 2) it is straight forward to link the strain and stress elements to the elastic compliance (S_{ij}) and elastic stiffness constants (C_{ij}), respectively as:

$$\varepsilon_{\parallel} = (S_{11} + 2S_{12})X + S_{12}P \tag{4a}$$

$$\varepsilon_{\perp} = (S_{11} + 2S_{12})X + S_{11}P \tag{4b}$$

$$X = (C_{11} + C_{12})\varepsilon_{\parallel} + C_{12}\varepsilon_{\perp} \tag{4c}$$

$$\text{and} \quad Z = 2C_{12}\varepsilon_{\parallel} + C_{11}\varepsilon_{\perp} \tag{4d}$$

Both compliance and stiffness tensors are related [51] through $\boldsymbol{S}=\boldsymbol{C}^{-1}$ for evaluating compliance coefficients (S_{11}, S_{12}, S_{44}) from the known elastic (C_{11}, C_{12}, C_{44}) constants. Again, the negative ratio of strains perpendicular and parallel to the stress axis is known as the

Poisson ratio ν. For the hydrostatic pressure, ν_H=-1 and for uniaxial stress along the *z*-axis ν_S=- $\varepsilon_{\parallel}/\varepsilon_{\perp}$.

If the zb crystal is deformed either internally (residual stress) or externally (applied stress) – the three optical phonon frequencies can be obtained by solving the secular equation [40]:

$$\begin{pmatrix} p\varepsilon_{xx}+q(\varepsilon_{yy}+\varepsilon_{zz})-\Delta\omega_i^2 & 2r\varepsilon_{xy} & 2r\varepsilon_{xz} \\ 2r\varepsilon_{xy} & p\varepsilon_{yy}+q(\varepsilon_{zz}+\varepsilon_{xx})-\Delta\omega_i^2 & 2r\varepsilon_{yz} \\ 2r\varepsilon_{xz} & 2r\varepsilon_{yz} & p\varepsilon_{zz}+q(\varepsilon_{xx}+\varepsilon_{yy})-\Delta\omega_i^2 \end{pmatrix}\begin{pmatrix} u_1 \\ u_2 \\ u_3 \end{pmatrix}=0 \quad (5)$$

where *p*, *q*, *r* are the symmetry allowed anharmonic parameters known as phonon deformation potentials. Here, the term $\Delta\omega_i^2(\equiv\omega_\varepsilon^2-\omega_o^2)$ $\left(\text{or } \omega_\varepsilon \approx \omega_o+\frac{\Delta\omega_i^2}{2\omega_o}\right)$ represents the shift of perturbed (strained: ω_ε^2) optical phonons from the unstrained $\vec{q}=0$ modes ω_o^2, and u_i are the components of eigen vectors. For axial stress with strains (Eq. 2) the non-trivial solutions of Eq. (5):

$$\begin{vmatrix} p\varepsilon_{xx}+q(\varepsilon_{yy}+\varepsilon_{zz})-\Delta\omega_i^2 & 2r\varepsilon_{xy} & 2r\varepsilon_{xz} \\ 2r\varepsilon_{xy} & p\varepsilon_{yy}+q(\varepsilon_{zz}+\varepsilon_{xx})-\Delta\omega_i^2 & 2r\varepsilon_{yz} \\ 2r\varepsilon_{xz} & 2r\varepsilon_{yz} & p\varepsilon_{zz}+q(\varepsilon_{xx}+\varepsilon_{yy})-\Delta\omega_i^2 \end{vmatrix}=0 \quad (6)$$

provide two phonon modes given by:

$$[p\varepsilon_{\parallel}+q(\varepsilon_{\parallel}+\varepsilon_{\perp})-\Delta\omega_i^2]^2[p\varepsilon_{\perp}+2q\varepsilon_{\parallel}-\Delta\omega_i^2]=0 \quad (7)$$

one having a doublet

$$\Delta\omega_{di}^2=p\varepsilon_{\parallel}+q(\varepsilon_{\parallel}+\varepsilon_{\perp})$$

$$\text{or } \omega_{d\varepsilon}=\omega_o+[(p+q)\varepsilon_{\parallel}+q\varepsilon_{\perp}]/2\omega_o \quad (8a)$$

and the other a singlet

$$\Delta\omega_{si}^2=p\varepsilon_{\perp}+2q\varepsilon_{\parallel}$$

$$\text{or } \omega_{s\varepsilon}=\omega_o+[p\varepsilon_{\perp}+2q\varepsilon_{\parallel}]/2\omega_o \quad (8b)$$

Stress induced modes: Hydrostatic case

In a hydrostatic case (*P*=0), with a_o changing to *a*: $\varepsilon_{xx}=\varepsilon_{yy}=\varepsilon_{zz}=\varepsilon=\frac{a-a_o}{a_o}$ and $\varepsilon_{ij}(i\neq j)=0$,

$$\begin{pmatrix} X \\ X \\ X \end{pmatrix}=\begin{pmatrix} C_{11} & C_{12} & C_{12} \\ C_{12} & C_{11} & C_{12} \\ C_{12} & C_{12} & C_{11} \end{pmatrix}\begin{pmatrix} \varepsilon \\ \varepsilon \\ \varepsilon \end{pmatrix} \quad (9a)$$

$$\text{or } X=(C_{11}+2C_{12})\varepsilon=\frac{C_{11}+2C_{12}}{3}\frac{\Delta V}{V_o}=B_o\frac{\Delta V}{V_o} \quad (9b)$$

where $\frac{\Delta V}{V_o}=(1+\varepsilon)^3-1\approx 3\varepsilon$ and $\frac{C_{11}+2C_{12}}{3}=B_o$ is the bulk modulus.

The Grüneisen constant (hydrostatic stress) γ_o is:

$$\gamma_o=-\frac{\partial\ln\omega}{\partial\ln V}=\frac{B_o}{\omega_o}\frac{\partial\omega}{\partial X} \quad (10)$$

where ω is the mode frequency and V_o crystal volume. By using Eqs. [8(a-b) and 10] one gets:

$$\frac{\Delta\omega}{\omega_o}=-\gamma_o\frac{\Delta V}{V_o}=-3\varepsilon\gamma_o=(p+2q)\varepsilon/2\omega_o^2 \quad (11)$$

where $\gamma_o=-(p+2q)/6\omega_o^2$.

If a cubic cell of lattice constant a_o is distorted to a tetragonal cell of lattice constants *a* and *c*, respectively, then $\varepsilon_{xx}=\varepsilon_{yy}=\varepsilon_{\parallel}=\frac{a-a_o}{a_o}$; $\varepsilon_{zz}=\varepsilon_{\perp}=\frac{c-a_o}{a_o}$ and $\varepsilon_{ij}(i\neq j)=0$. Consequently, one can rewrite Eqs. [8(a)-(b)] as:

$$\frac{\Delta\omega_{di}^2}{\omega_o^2}=[p\varepsilon_{\parallel}+q(\varepsilon_{\parallel}+\varepsilon_{\perp})]/\omega_o^2=\frac{(p+2q)}{3\omega_o^2}(2\varepsilon_{\parallel}+\varepsilon_{\perp})+\frac{(p-q)}{3\omega_o^2}(\varepsilon_{\parallel}-\varepsilon_{\perp}),$$

$$\text{or}=-2\gamma_o(2\varepsilon_{\parallel}+\varepsilon_{\perp})+\frac{2}{3}\gamma_s(\varepsilon_{\parallel}-\varepsilon_{\perp}), \quad (12)$$

$$\text{and } \frac{\Delta\omega_{si}^2}{\omega_o^2}=[p\varepsilon_{\perp}+2q\varepsilon_{\parallel}]/\omega_o^2=\frac{(p+2q)}{3\omega_o^2}(2\varepsilon_{\parallel}+\varepsilon_{\perp})-2\frac{(p-q)}{3\omega_o^2}(\varepsilon_{\parallel}-\varepsilon_{\perp})$$

$$\text{or}=-2\gamma_o(2\varepsilon_{\parallel}+\varepsilon_{\perp})-\frac{4}{3}\gamma_s(\varepsilon_{\parallel}-\varepsilon_{\perp}), \quad (13)$$

where $\gamma_s=\frac{(p-q)}{2\omega_o^2}$ is the shear-deformation parameter.

Stress induced modes: Uniaxial case

If a uniaxial stress is applied in the *z*-direction:

$$\begin{pmatrix} 0 \\ 0 \\ P \end{pmatrix}=\begin{pmatrix} C_{11} & C_{12} & C_{12} \\ C_{12} & C_{11} & C_{12} \\ C_{12} & C_{12} & C_{11} \end{pmatrix}\begin{pmatrix} \varepsilon_{\parallel} \\ \varepsilon_{\parallel} \\ \varepsilon_{\perp} \end{pmatrix} \quad (14)$$

one gets:

$$(C_{11}+C_{12})\varepsilon_{\parallel}+C_{12}\varepsilon_{\perp}=0 \quad (15a)$$

$$\text{and } 2C_{12}\varepsilon_{\parallel}+C_{11}\varepsilon_{\perp}=P \quad (15b)$$

Solving the above two Eqs. [15(a)-(b)], it can be shown that:

$$2\varepsilon_{\parallel}+\varepsilon_{\perp}=\frac{P}{C_{11}+2C_{12}} \quad (15c)$$

$$\text{and } \varepsilon_{\parallel}-\varepsilon_{\perp}=\frac{P}{C_{11}-C_{12}} \quad (15d)$$

Substituting Eqs. [15(c-d)] into Eqs. [(12) and (13)] one can obtain

$$\frac{\omega_{d\varepsilon}^2-\omega_o^2}{\omega_o^2}=-2\gamma_o\frac{P}{C_{11}+2C_{12}}+\frac{2}{3}\gamma_s\frac{P}{C_{11}-C_{12}}, \quad (16a)$$

$$\text{and } \frac{\omega_{s\varepsilon}^2-\omega_o^2}{\omega_o^2}=-2\gamma_o\frac{P}{C_{11}+2C_{12}}-\frac{4}{3}\gamma_s\frac{P}{C_{11}-C_{12}}, \quad (16b)$$

Subtracting Eqs. [16(a)-(b)], we will have

$$\frac{\omega_{s\varepsilon}^2-\omega_{d\varepsilon}^2}{\omega_o^2}=-2\gamma_s\frac{P}{C_{11}-C_{12}} \quad (17a)$$

$$\frac{\omega_{s\varepsilon}^2+2\omega_{d\varepsilon}^2-3\omega_0^2}{\omega_o^2}=-6\gamma_0\frac{P}{C_{11}+2C_{12}} \quad (17b)$$

$$\text{or } \frac{3\omega_h^2-3\omega_0^2}{\omega_o^2}=-6\gamma_0\frac{P}{C_{11}+2C_{12}}$$

$$\frac{\omega_h^2-\omega_0^2}{\omega_o^2}=-2\gamma_0\frac{P}{C_{11}+2C_{12}}=-\frac{2\gamma_0}{3B_0}P \quad (17c)$$

where we defined $\omega_{s\varepsilon}^2+2\omega_{d\varepsilon}^2=3\omega_h^2$

Stress induced modes: Biaxial case

The 3C-SiC/Si(001) system is regarded as one with biaxial stress

(i.e., P=-X : cf. Eq. 3) in the film due to difference in the substrate lattice constants and thermal expansion coefficients. With Eq. [4 (d)], one can rewrite Eqs. [8(a)-(b)] as

$$\omega_{d\varepsilon} = \omega_o + [(p+q)\varepsilon_{\parallel} + q\varepsilon_{\perp}]/2\omega_o = \omega_o + \left[\left(\frac{p+q}{2\omega_o}\right) - \left(\frac{qC_{12}}{\omega_o C_{11}}\right)\right]\varepsilon_{\parallel}$$

$$= \omega_o + \omega_o\left[\frac{1}{3}\gamma_s\left(1+\frac{2C_{12}}{C_{11}}\right) + 2\gamma_o\left(\frac{C_{12}}{C_{11}}-1\right)\right]\varepsilon_{\parallel} \qquad (18a)$$

$$= \omega_o + \omega_o\left[\frac{1}{3}\gamma_s(S_{11}-S_{12}) - 2\gamma_o(S_{11}+2S_{12})\right]X$$

$$= \omega_o + \left[\frac{1}{3}\zeta_S - 2\zeta_H\right]X$$

$$\omega_{s\varepsilon} = \omega_o + [p\varepsilon_{\perp} + 2q\varepsilon_{\parallel}]/2\omega_o = \omega_o + \left[\left(\frac{q}{\omega_o}\right) - \left(\frac{pC_{12}}{\omega_o C_{11}}\right)\right]\varepsilon_{\parallel}$$

and $$= \omega_o + \omega_o\left[-\frac{2}{3}\gamma_s\left(1+\frac{2C_{12}}{C_{11}}\right) + 2\gamma_o\left(\frac{C_{12}}{C_{11}}-1\right)\right]\varepsilon_{\parallel}$$

$$= \omega_o + \omega_o\left[-\frac{2}{3}\gamma_s(S_{11}-S_{12}) - 2\gamma_o(S_{11}+2S_{12})\right]X$$

or $$= \omega_o + \left[-\frac{2}{3}\zeta_S - 2\zeta_H\right]X \qquad (18b)$$

where the two stress coefficients

$$\zeta_S = \omega_o\gamma_S(S_{11}-S_{12}) \text{ and } \zeta_H = \omega_o\gamma_o(S_{11}+2S_{12}) \qquad (19)$$

can be determined by RS experiments. Again it is customary to add superscripts TO, LO on ω, ω_o for classifying the doublet and singlet (cf. Eqs. 18(a-b)) modes i.e.,

$$\omega^{TO} = \omega_o^{TO} + \left[\frac{1}{3}\zeta_S - 2\zeta_H\right]X \qquad (20a)$$

$$\omega^{LO} = \omega_o^{LO} + \left[--\zeta_S - 2\zeta_H\right]X \qquad (20b)$$

Subtracting Eq. (20 a) from Eq. (20 b) one can obtain $\zeta_S X$:

$$\zeta_S X = (\omega_o^{LO} - \omega^{LO}) - (\omega_o^{TO} - \omega^{TO}), \qquad (21)$$

from the observed Raman mode frequencies ($\omega^{LO}, \omega^{TO}, \omega_o^{LO}$ and ω_o^{TO}). Using Eq. (21) with hydrostatic stress coefficients ζ_H^{LO}, ζ_H^{TO} known from the pressure dependent RS experiments, we can get two values of X from Eqs. [20(a-b)]:

$$X = [(\omega_o^{TO} - \omega^{TO}) + \frac{1}{3}\zeta_S X]/(2\zeta_H^{TO}) \qquad (22)$$

and $$X = [(\omega_o^{LO} - \omega^{LO}) - \frac{2}{3}\zeta_S X]/(2\zeta_H^{TO}) \qquad (23)$$

If we take an average of the two X values and assign error bar, we can appraise both in-plane and normal strains in 3C-SiC films by using Eqs. [4(a)-(b)] and setting P=-X. It is to be noted that the classical elastic deformation theory assumes a linear relationship between stress and strain (Eqs. (10 and 15-17)) – which may not be very realistic at higher X>10 GPa. In our analyses from RSS data of optical phonons the estimated values of hydrostatic pressure components are seen to fall well within X<1 GPa in all V-CVD grown 3C-SiC/Si (001) samples. It is, therefore, strongly believed that in the elastic deformation theory one would anticipate nearly <5% error in assessing strains.

Results: Data Analysis

Elastic constants

Accurate knowledge of elastic constants for 3C-SiC is crucial for engineering MEMS and/or NEMS devices and evaluating stress and strains in 3C-SiC/Si (001) epilayers (Eqs. (4a-b)). The published data on elastic constants by exploiting diverse experimental and theoretical methods is, however, rather conflicting [52-66]. The complete result on lattice dynamics of 3C-SiC has been reported earlier[67] by inelastic x-ray scattering (IXS) method. The pressure dependent optical phonon shifts in bulk 3C-SiC crystals are investigated with applied hydrostatic pressure (X) up to 22.5 GPa [37]. Recently, we have adopted a realistic rigid-ion model (RIM) to simulate phonon dispersions of 3C-SiC at 1 atm [31] and 22.5 GPa [67]. In the RIM scheme, the short- and long-range Coulomb interactions are optimized by least-square fitting procedures using lattice constants, critical point phonon energies as input while elastic constants C_{ij} and their pressure derivatives are deliberated as constraints to match the IXS [67] and pressure-dependent phonon data. For 3C-SiC, the best fit values of phonon dispersions find recent experimental [54] and local density functional data of elastic constants more reliable than the results available from earlier measurements. In Table 2 we have listed the derived values of elastic compliances (S_{11}, S_{12}, S_{44}), S_{11}+2S_{12}, $\tilde{S}$ and Poisson ratio ν_s, from elastic constants (C_{11}, C_{12}, C_{44}) reported [52-66] by various research groups.

Grüneisen parameter

Earlier, Olego et al. [36,37] described the hydrostatic pressure dependent optical [$\omega_{LO(\Gamma)}$, $\omega_{TO(\Gamma)}$] phonons in bulk 3C-SiC crystals by using RSS with applied X up to 22.5 GPa:

$$\omega^{TO} = (796.2 \pm 0.3) + (3.88 \pm 0.08)\,X - (2.2 \pm 0.4) \times 10^{-2}\,X^2 \qquad (24a)$$

$$\omega^{LO} = (972.7 \pm 0.3) + (4.75 \pm 0.09)\,X - (2.5 \pm 0.4) \times 10^{-2}\,X^2 \qquad (24b)$$

where the mode frequencies ω^{TO}, ω^{LO} are expressed in cm^{-1} while X is in GPa (10^{10} dyn/cm^2). For 3C-SiC, the optical phonon shifts at low temperature (6 K) have also been reported with X up to 15 GPa [42]. In Figure 3, a linear fit to the phonon data by dotted lines has revealed that for X<10 GPa the X^2 term in the right hand side of Eqs. (24a-b) is trivial and can be neglected. Therefore, one can determine the hydrostatic Grüneisen parameters γ_H^{TO}, γ_H^{LO} from the linear relationship (Eq. (10))

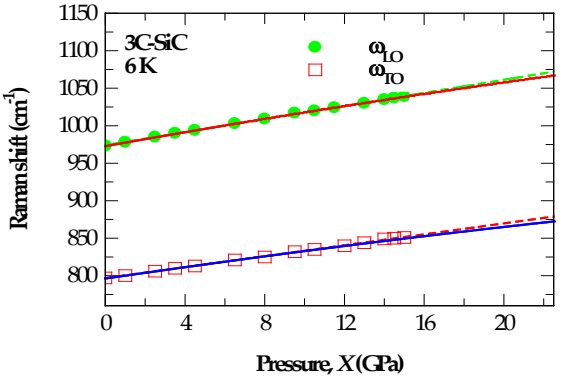

Figure 3: The long wavelength $\omega_{LO(\Gamma)}$, $\omega_{TO(\Gamma)}$ phonon mode frequencies of 3C-SiC vs. hydrostatic pressure (GPa). The symbols (●, □) represent experimental data [42] whereas the solid lines correspond to the data fits and dashed lines represent the linear fit to the experimental results.

3C-SiC									
c_{11}	c_{12}	c_{44}	s_{11}	s_{12}	s_{44}	$s_{11}+2s_{12}$	$\hat{s}$	v_s	Ref.
($x*10^{12}$ dyn/cm^2)			($x*10^{-13}$ cm^2/dyn)			($x*10^{-13}$ cm^2/dyn)			
5.4	1.8	2.5	2.222	-0.556	4	1.111	2.5	0.25	[52] Exp.
3.9	1.42	2.56	3.183	-0.85	3.906	1.484	2.718	0.267	[53] Exp.
3.95	1.36	2.36	3.074	-0.787	4.237	1.499	2.575	0.256	[54] Exp.
3.523	1.404	2.329	3.673	-1.047	4.294	1.58	2.988	0.285	[55] Cal.
3.489	1.384	2.082	3.7	-1.051	4.803	1.598	2.972	0.284	[56] Cal.
3.71	1.69	1.76	3.77	-1.18	5.682	1.41	3.51	0.313	[57] Cal.
2.89	2.34	0.554	12.56	-5.62	18.05	1.321	13.764	0.447	[58] Cal.
3.9	1.426	1.911	3.188	-0.854	5.233	1.481	2.729	0.268	[59] Cal.
4.2	1.26	2.87	2.764	-0.638	3.484	1.488	2.286	0.231	[60] Cal.
3.9	1.34	2.53	3.111	-0.795	3.953	1.52	2.57	0.256	[61] Cal.
4.05	1.35	2.54	2.963	-0.741	3.937	1.481	2.5	0.25	[62] Cal.
4.2	1.2	2.6	2.727	-0.606	3.846	1.515	2.2	0.222	[63] Cal.
3.84	1.32	2.41	3.16	-0.808	4.149	1.543	2.571	0.256	[64] Cal.
4.151	1.319	2.654	2.845	-0.686	3.768	1.473	2.397	0.241	[65] Cal.
3.63	1.54	1.49	3.687	-1.098	6.711	1.49	3.211	0.298	[66] Cal.

Table 2: Calculated elastic compliance and other parameters of 3C-SiC obtained from the existing sets of elastic constants available in the literature.

	ω_0 (cm^{-1})	dω/dX	γ_o	B (GPa)	B
3C-SiC[a]	TO(Γ) 797.7	3.88	1.56,b 1.10[c]	227	4.1
	LO(Γ) 973.6	4.59	1.55,b 1.09[c]		
	LO-TO 175.9	0.654			
C (dia)[a]	1330	2.9	0.96	442	4.09
Si	523.9	5.1	0.96	99	4.24
Ge	304.6	4.02	1	75.8	4.55

[a]Ref. [42].
[b]Ref. [36-37].
[c]Our

Table 3: Zone-center optical phonon frequencies [TO(Γ), LO(Γ)] and their hydrostatic pressure derivatives dω/d*X* for 3C-SiC. The phonon frequencies ω_o are in cm^{-1} and the hydrostatic pressure *X* is in GPa. For comparison we have listed the related data for zone-center modes [ω_o (cm^{-1})] of diamond, Si, and Ge crystals. The mode Grüneisen parameters γ_o, the bulk moduli B (in GPa) and their pressure derivatives B′ employed to calculate $\frac{\Delta V}{V_o}$ or $\frac{\Delta a}{a_o}$ for 3C-SiC are also listed.

Sample #	d_{SiC} μm	ω_o^{TO} cm^{-1}	ω_o^{LO} cm^{-1}	ω^{TO} cm^{-1}	ω^{LO} cm^{-1}	X(GPa)	$\varepsilon_{\parallel}$ (%)	$\varepsilon_{\perp}$ (%)	Ref.
125 A	2.4	795.5	972.8	794.2	971.6	0.446 ± 0.045	0.102	-0.072	[our]
119 A	3.2	795.7	972.9	793.9	971.8	0.552 ± 0.056	0.126	-0.087	[our]
119 B	9.6	795.8	973.2	793.5	971.5	0.739 ± 0.075	0.169	-0.116	[our]
113	12.8	796	973.4	793.3	971.4	0.868 ± 0.088	0.199	-0.137	[our]
487*	4	795.5	972.4	794.3	969.9	0.575 ± 0.058	0.132	-0.091	[41]
475 B	4.5	795.1	972.4	793.1	971.1	0.622 ± 0.063	0.142	-0.098	[41]
462	6	796.3	973.6	793.1	970.3	1.138 ± 0.115	0.26	-0.179	[41]
475	7	796.3	972.8	794.3	969.9	0.810 ± 0.082	0.185	-0.127	[41]

Table 4: Comparison of the Raman scattering data on optical phonons (cm^{-1}) used for assessing the stresses and strains in V-CVD grown 3C-SiC/Si (001). We used elastic compliance values of S_{11}=3.074 × 10^{-13} cm^2/dyn and S_{12}=-0.787 × 10^{-13} cm^2/dyn (Table 3) from the experimental data of elastic constants [54].

involving $\frac{\partial\omega}{\partial X}$. For 3C-SiC, the values [$\gamma_H^{TO}=1.56,\ \gamma_H^{LO}=1.55$] estimated by Olego et al. used an average bulk modulus data B_o (=321.9 GPa) of Si and C (Table 3) [36,37]. A correction was made to the γ_H^{TO}, γ_H^{LO} values by exploiting the experimental bulk modulus B_o (=227 GPa) of 3C-SiC. While the experimental results of hydrostatic mode Grüneisen parameters for 3C-SiC fall within <3% – our RIM calculations [67] of $\gamma_H^{TO}=1.1,\ \gamma_H^{LO}=1.09$ provided strong corroborations to the amended values. While Feng et al. [41] employed $\gamma_H^{TO}=1.56,\ \gamma_H^{LO}=1.55$ for assessing strains in 3C-SiC epifilms – one would expect improvement in the strain values if accurate results of γ_H^{TO}, γ_H^{LO} are adopted.

Stress and strain in V-CVD 3C-SiC/Si (001) films

In Table 4 we have displayed the RSS results of optical phonons ω^{LO}, ω^{TO} and $\omega_o^{LO}, \omega_o^{TO}$ in the near-backscattering geometry for several "as-grown" 3C-SiC/Si (001) and "free-standing" films. By using Eqs. [(21) and (22-23)] along with the Raman data of optical phonons and hydrostatic stress coefficients ζ_H^{TO}, ζ_H^{TO} we obtained two values of *X* – took their average result and assigned an error bar (Table 4). From Table 4, the uncertainty of the calculated stress *X* is about 10% which agrees very well with the estimated value from the experimental error of 10% to 20% from the pressure dependent RSS mode frequencies. The results of in-plane and normal strains are evaluated for 3C-SiC films by exploiting Eqs. [4(a)-(b): setting *P*=-*X*] along with the elastic compliance data of S_{11}=3.074x10^{-13} cm^2/dyn and S_{12}=-0.787x10^{-13} cm^2/dyn from Table 2 [54]. The calculated values reported in Table 4 of biaxial stress (*X*~0.45-0.87 GPa) and inplane ($\varepsilon_{\perp}$ ~0.1-0.2%) strains as well as normal ($\varepsilon_{\parallel}$~-0.07 to -0.14%) strains for several V-CVD grown

samples of different thickness are found in good agreement with the results reported in the literature. The positive and negative signs of $\varepsilon_{\parallel}$ and $\varepsilon_{\perp}$ indicate that in-plane strains are tensile while the normal strains are compressive respectively for all 3C-SiC/Si (001) samples. In order to justify the use of elastic deformation theory for 3C-SiC films, we have studied the volume dependent shifts of optical phonons by using a well known Murnaghan's equation of state with B_o (≡227 GPa) and B_o' (≡4.1):

$$\frac{\Delta V}{V_o} = \left[1 + X\frac{B_o'}{B_o}\right]^{-1/B_o'} - 1 \quad . \tag{25}$$

The results displayed in Figure 4 for small X clearly reveal a linear dependence of the relative change for $\frac{\Delta\omega^{LO}}{\omega^{LO}}\left\{\approx\frac{\Delta\omega^{TO}}{\omega^{TO}}\right\}$ versus $\frac{\Delta V}{V_o}$ as compared to non-linear behavior of the hydrostatic pressure X>10 GPa dependent shifts for optical modes ω^{LO}, ω^{LO} (Figure 3). This means that for X>10 GPa, the deviation from a linear behavior of pressure dependent mode frequencies ω^{LO}, ω^{TO} (Figure 3) is caused by the non-linear pressure – volume relationship. In other words if X^2 terms from the right-hand side of Eqs. (24a-b)) are neglected – one would expect nearly ~5% error in the optical mode frequencies for X>10 GPa and less than 0.5% for X<1 GPa. This result is quite significant as the evaluated hydrostatic pressure component X in all V-CVD grown 3C-SiC/Si (001) samples are found to be <1 GPa – validateing our elastic deformation theory of assessing strains in epifilms grown on mismatched substrates.

Summary and Conclusion

In summary, we have carried out extensive RSS measurements on several highly mismatched thin epitaxially grown 3C-SiC films on thick Si (001) substrates using V-CVD method. The 3C-SiC/Si (001) material system is perceived as one with a biaxial stress due to differences in the lattice constants and thermal expansion coefficients. In the V-CVD approach, while keeping Si/C ratio at ~0.33 we have prepared 3C-SiC films on Si by varying the growth time between 2 min to 4 h. A conventional elastic deformation theory is used to derive the necessary expressions involving stress coefficients – correlating them with Raman phonon shifts and hydrostatic, uniaxial and biaxial stresses. For bulk 3C-SiC, we used the existing pressure dependent phonon [37,42] measurements to estimate the hydrostatic-stress coefficients. The experimental data of long wavelength optical phonons [LO(Γ) and TO(Γ)] in the near-backscattering geometry is compared for several "as-grown" 3C-SiC/Si (001) and "free-standing" samples having film thickness ranging between 2.4 μm to 12.8 μm. The analysis of Raman scattering phonon data has not only helped us appraise the crystalline quality of films but also facilitated assessing the stresses and strains in several V-CVD grown 3C-SiC/Si (001) samples of different thickness. Our estimated results of biaxial stresses (X~0.45-0.87 GPa) as well as inplane ($\varepsilon_{\parallel}$ ~0.1–0.2%) and normal ($\varepsilon_{\perp}$ ~-0.07 to -0.14%) strains using elastic deformation theory with elastic constants from Philippe Djemia provided values in good agreement with data reported in the literature by different research groups [41,44]. In 3C-SiC/Si epifilms, while the appraised average value of the biaxial stress (~0.651 GPa) is an order of magnitude smaller – the strain estimates are found two-order of magnitudes smaller than the lattice misfits between the bulk 3C-SiC and Si. Although this result is quite interesting – it provides strong corroboration to our recent study of impurity vibrational modes based on average-t-matrix Green's function theory implying that there exists a high density of intrinsic defects at the 3C-SiC/Si interface which is possibly responsible for releasing misfit stresses and strains.

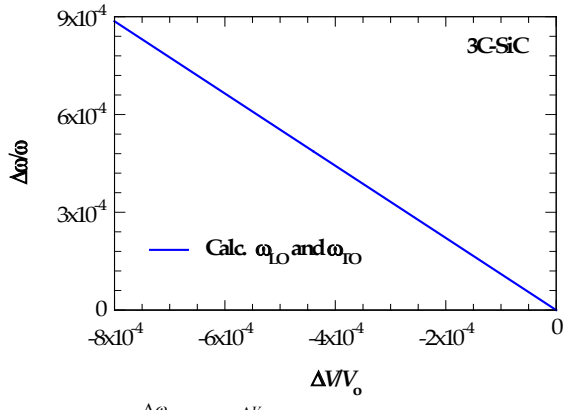

Figure 4: Plot of $\frac{\Delta\omega}{\omega}$ versus $\frac{\Delta V}{V_o}$ for the strained 3C-SiC grown on Si (001) substrate.

Acknowledgements

The author (DNT) wishes to thank Dr. Deanne Snavely, Dean College of Natural Science and Mathematics at Indiana University of Pennsylvania for the travel support and the Innovation Grant that he received from the School of Graduate Studies making this collaborative research possible. The work at Guangxi University is supported by National Natural Science Foundation of China (NO. 61367004) and Guangxi Key Laboratory for the Relativistic Astrophysics-Guangxi Natural Science Creative Team funding (No. 2013GXNSFFA019001).

References

1. Zhuang H, NYang N, Zhang L, Fuchs R, Jiang X (2015) Low-Temperature Non-Ohmic Galvanomagnetic Effects in Degenerate n-Type InAs. ACS Appl Mater Interfaces 7: 10886-10895.
2. Frewin CL, Reyes M, Register J, Thomas SW, Saddow SE (2014) 3C-SiC on Si: A Versatile Material for Electronic, Biomedical and Clean Energy Applications. MRS Proceedings 1693: dd05-01.
3. Choi K, Choi DK, Lee DY, Shim J, Ko S (2012) Nanostructured thermoelectric cobalt oxide by exfoliation/restacking route. Appl Phys 108: 161.
4. Rajasekhara S, Neuner BH, Zorman CA, Jegenyes N, Ferro G, et al. (2011) Mixed-Mode Excitons in the Photoluminescence of Zinc Oxide-Reabsorption and Exciton Diffusion. Appl Phys Lett 98: 191904.
5. Yang N, Zhuang H, Hoffmann R, Smirov W, Hess J, et al. (2011) Growth and Characterization of 3C-SiC Films for Micro Electro Mechanical Systems (MEMS) Applications. Anal Chem 83: 5827.
6. Bosi M, Watts BE, Attolini G, Ferrari C, Frigeri C, et al. (2009) Growth and Characterization of 3C-SiC Films for Micro Electro Mechanical Systems (MEMS) Applications. Cryst Growth Design 9: 4852.
7. Reddy JD, Volinsky AA, Frewin CL, Locke C, Saddow SE (2008) Quantum Theory of a Basic Light-Matter Interaction. Mater Res Soc Symp Proc 1049: AA03-06.
8. Young DJ, Du J, Zorman CA, Ko WH (2004) Effects of Uniaxial Stress on Excitons in CuCl. IEEE Sensors 4: 464.
9. Baliga BJ (2005) Silicon Carbide – Power Devices. World Scientific, Singapore.
10. Neudeck PG (2003) VLSI Technology (Ed. Wai-Kai Chen). CRC Press, USA.
11. Choyke WJ, Matsunami H, Pensl G (2004) Silcon carbide: Recent Major Advances (Springer-Verlag, Berlin, USA.
12. Saddow SE, Agarwal A (2004) Advances in Silicon carbide - Processing and Applications. Artech House, Inc. Boston.
13. Feng ZC (2004) SiC Power Materials-Devices and Applications. Springer, Berlin.
14. Feng ZC, Zhao JH (2003) Silicon Carbide: Materials, Processing and Devices. Taylor & Francis Books Inc, New York.
15. Phan HP, Dinh T, Kozeki T, Qamar A, Namazu T, et al. (2016) Triply Differential Cross Sections for the Ionization of Helium by Fast Electrons. Scientific Reports 6: 28499.

16. Wijesundara MBJ, Azevedo R (2011) Silicon Carbide Microsystems for Harsh Environments. Springer-Verlag New York.
17. Scaburri R (2011) The incomplete ionization of substitutional dopants in silicon carbide, Dottorato di Ricerca in Ingegneria dei Materiali, Universitá di Bologna, Italy.
18. Rurali R, Godignon P, Rebollo J,Hernández E, Ordejón P (2003) Spectrum of Small-Scale Density Fluctuations in Tokamaks. Appl Phys Lett 82: 4298.
19. Liu P (2014) Atomic Structure of the Vicinal Interface between Silicon Carbide and Silicon Dioxide. The University of Tennessee, Knoxville.
20. Gupta SK, Akhtar J (2011) Thermal Oxidation of Silicon Carbide (SiC) – Experimentally Observed Facts. Intech 1-26.
21. Hornos T (2008) Theoretical study of defects in silicon carbide and at the silicon dioxide Interface. Budapest University of Technology and Economics, USA.
22. Fu W (2015) Design and Comparison of Si-based and SiC-based Three-Phase PV Inverters. The University of Wisconsin-Milwaukee, USA.
23. Nawaz M (2015) Active and Passive Electronic Components 651527.
24. Shibahara K, Kuroda N, Nishino S, Matsunami H (1987) Magnetic Double Transition in Au-Fe near the Percolation Threshold. Jpn J Appl Phys 26: L1815.
25. Kong HS, Glass JT, Davis RF (1988) Direct Determination of Sizes of Excitations from Optical Measurements on Ion-Implanted GaAs. J Appl Phys 64: 2672.
26. Powell JA, Larkin DJ, Matus LG, Choyke WJ, Bradshaw JL, et al. (1990) Localized Modes and Cell-Model Limit in the Crystal Impurity Problem. Appl Phys Lett 56: 1442.
27. Nishino K, Kimoto T, Matsunami H (1995) Thermally Stimulated Exoelectron Emission. Jpn J Appl Phys 34: L1110.
28. Kimoto T, Yamashita A, Itoh A, Matsunami H (1993) Domain walls and ferroelectric reversal in corundum derivatives. Jpn J Appl Phys 32: 1045.
29. Steckl AJ, Roth MD, Powell JA, Larkin DJ (1993) Numerical analytic continuation: Answers to well-posed questions. Appl Phys Lett 62: 2545.
30. Tin CC, Hu R, Williams J, Feng ZC, Yue KT (1994) Origin of the second peak in the mechanical loss function of amorphous silica. Mat Res Soc Symp 339: 411.
31. Talwar DN (2015) Non-Hermitian bidirectional robust transport. Diamond and Related Mater 52: 1.
32. Park JH, Kim JH, Kim Y, Lee BT, Jang SJ, et al. (2003) Intrinsic localized mode and low thermal conductivity of PbSe. Appl Phys Lett 83: 1989.
33. Anzalone R, Locke C, Carballo J, Piluso1 N, Severino A, et al. (2010) Critical behavior in the presence of an order-parameter pinning field. Mat Sci Forum 143: 645-648.
34. Anastassakis E, Pinczuk A, Burstein E, Pollak FH, Cardona M (1970) Efficient spin transport through polyaniline. Solid State Commun 8: 133.
35. Cerdeira F, Buchenauer CJ, Pollak FH, Cardona M (1971) Stress-Induced Shifts of First-Order Raman Frequencies of Diamond- and Zinc-Blende-Type Semiconductors. Phys Rev B: 580.
36. Olego D, Cardona M (1982) Pressure dependence of Raman phonons of Ge and 3C-SiC. Phys Rev B 25: 1151.
37. Olego D, Cardona M, Vogl P (1982) Pressure dependence of the optical phonons and transverse effective charge in 3C-SiC. Phys Rev B 25: 3878.
38. Jusserland B, Voisin P, Voos M, Chang LL, Mendez EE, et al. (1985) Advances in quantitative Kerr microscopy. Appl Phys Lett 46: 678.
39. Shon LH, Inoue K, Murase K (1987) Dynamics of skyrmionic states in confined helimagnetic nanostructures. Solid State Commun 62: 621.
40. Mukaida H, Okumura H, Lee JH, Daimon H, Sakuma E, et al.(1987) Raman scattering of SiC: Estimation of the internal stress in 3C-SiC on Si. J Appl Phys 62: 254.
41. Feng ZC, Mascarenhas AJ, Choyke W, Powell JA (1988) Optical conductivity from pair density waves. J Appl Phys 64: 3178.
42. Debernardi A, Ulrich C, Cardona M, Syassen K (2001) Pressure Dependence of Raman Linewidth in Semiconductors. Phys Stat Sol 223: 213.
43. Zhuravlev KK, Goncharov AF, Tkachev SN, Dera P, Prakapenka VB (2013) Vibrational, elastic, and structural properties of cubic silicon carbide under pressure up to 75 GPa: Implication for a primary pressure scale. J Appl Phys 113: 113503.
44. Zhu J, Liu S, Lia W (2000) Large-scale normal fluid circulation in helium superflows. Thin Solid Films 368: 307.
45. Capano MA, Kim BC, Smith AR, Kvam EP, Tsoi S, et al. (2006) Time Resolved Spectroscopy of Defects in SiC. J Appl Phys 100: 08514.
46. Shafiq M, Subhash G (2014) Thermoluminescence and Related Electronic Processes of 4H/6H-SiC. Experimental Mechanics 54: 763.
47. Harima H (2002) Properties of GaN and related compounds studied by means of Raman scattering. J Phys: Condens Matter 14: R967-R993.
48. Nakashima S, Harima H (1997) Raman Investigation of SiC Polytypes. Phys Stat Solidii A162: 39-64.
49. Nye JF (1957) Physical properties of crystals. Oxford Univ Press, London.
50. Lekhnitskii SG (1963) Theory of elasticity of an anisotropic elastic body. Holden-Day.
51. Bower AF (2010) Applied mechanics of solids. Taylor and Francis Group, CRC Press, USA.
52. Slack GA (1964) Advances in SiC MOS Technology. J Appl Phys 35: 3460.
53. Feldman DW, Parker JH, Choyke WJ, Patrick L (1968) High Temperature Sensors Based on Metal–Insulator–Silicon Carbide Devices. Phys Rev 173: 787.
54. Djemia P, Roussigné Y, Dirras GF, Jackson KM (2004) Optical Characterization of Silicon Carbide Polytypes. J Appl Phys 95: 2324.
55. Tolpygo KB (1961) High Pressure Synthesis of Binary B–S Compounds. Sov Phys-Solid State 2: 2367.
56. Miura M, Murata H, Shiro Y, Lishi K (1981) Control of Electronic Properties of Organic Conductors by Hydrostatic and Uniaxial Compression. J Phys Chem Solids 42: 931.
57. Lee DH, Joannopoulos JD (1982) Simple Scheme for Deriving Atomic Force Constants: Application to SiC. Phys Rev Lett 48: 1846.
58. Marshall RC, Faust JW, Ryan CE (1974) Silicon Carbide. University of South Carolina, Columbia, SC.
59. Vashishtha P, Kalia RK, Nakano A, Rino JP (2007) Interaction potential for silicon carbide: A molecular dynamics study of elastic constants and vibrational density of states for crystalline and amorphous silicon carbide. J Appl Phys 101: 103515.
60. Lambrecht WRL, Segall B, Methfessel M, van Schilfgaarde M (1991) Calculated elastic constants and deformation potentials of cubic SiC. Phys Rev B44: 3685.
61. Karch K, Pavone P, Mindi W, Schutt O, Strauch D (1994) Ab initio calculation of structural and lattice-dynamical properties of silicon carbide. Phys Rev B 50: 17054.
62. Li W, Wang T (1999) Elasticity, stability, and ideal strength of β-SiC in plane-wave-based ab initio calculationsPhys Rev B 59: 3993.
63. Teroff J (1989) Modeling solid-state chemistry: Interatomic potentials for multicomponent systems. Phys Rev B 39: 5566.
64. Wang CZ, Rici Yu, Krakauer H (1996) Pressure dependence of Born effective charges, dielectric constant, and lattice dynamics in SiC. Phys Rev B 53, 5430.
65. Yu-Ping L, Duan-Wei H, Jun Z, Xiang Dong Y (2008) Effects of Confinement on the Coupling between Nitrogen and Band States in InGaAs1-xNx/GaAs (x ≤ 0.025) Structures: Pressure and Temperature Studies. Phys B 43: 3543.
66. Lee DH, Joannopoulos JD (1982) Simple Scheme for Deriving Atomic Force Constants: Application to SiC. Phys Rev Lett 48: 1846.
67. Serrano J, Strempfer J, Cardona M, Schwoerer-Böhning M, Requardt H, et al. (2002) High Pressure Studies of the Raman-Active Phonons in Carbon Nanotubes. Appl Phys Lett 80: 4360.

Citation: Talwar DN, Wan L, Tin CC, Feng ZC (2017) Assessing Biaxial Stress and Strain in 3C-SiC/Si (001) by Raman Scattering Spectroscopy. J Material Sci Eng 6: 324. doi: 10.4172/2169-0022.1000324